Thermal and mechanical limitations to processing resolution in volume non-diffractive ultrafast laser structuring

Guodong Zhang, Razvan Stoian, Rui Lou, Tianqu Chen, Guangying Li, Xu Wang, Yan Pan, Pengfei Wu, Jiang Wang, Guanghua Cheng

Thermal and mechanical limitations to processing resolution in volume non-diffractive ultrafast laser structuring

Guodong Zhang [a], Razvan Stoian [b], Rui Lou [a], Tianqu Chen [a], Guangying Li [a], Xu Wang [a], Yan Pan [a], Pengfei Wu [a], Jiang Wang [a], and Guanghua Cheng [a,*]

[a] *School of Electronics and Information, School of Artificial Intelligence, Optics and Electonics, Northwestern Polytechnical University, Xi'an 710072, China*

[b] *Laboratoire Hubert Curien, UMR 5516 CNRS, Université Jean Monnet, 42000 Saint Etienne, France*

**Corresponding author: guanghuacheng@nwpu.edu.cn*

Received XX Month XXXX; Revised XX Month, XXXX; Accepted XX Month XXXX; Available online XX Month XXXX (Doc. ID XXXXX)

The minimum feature size and spatial resolution are key factors for ultrafast laser structuring, defining the resulting function of the structured material. With the aim to improve the processing resolution achievable for non-diffractive beams, we analyze in volume the hydrodynamic and thermomechanical material responses during laser structuring defining the affected zone. The extent of laser induced cavitation on a 100 nm scale, accompanied by local annealing,-and internal fracture under stress on μm scale are revealed using a combination ion beam milling, chemical etching and electron microscopy. Melting and mechanical stress acting at different planes are proved to be primary factors for restricting the structuring resolution to a critical distance where cooperative effects appear. Their extent is controllable via the local intensity and, hence, the pulse duration. A parametric control on the accumulated energy density limiting the thermomechanical action range and maximizing resolution is then reported.

KEYWORDS: ultrafast laser processing, surface and internal nanostructures, thermodynamics, laser-matter interaction processes

1. INTRODUCTION

Ultrafast laser processing is nowadays a flexible, non-contact and precise structuring technology for a range of applications in micro and nanotechnologies. Its accuracy sparked a great deal of interest for rapid development of structured materials and functions resulting from small feature sizes and their spatial order. With a capability to reach intensities in the TW/cm^2 range at the focal point and to trigger extremely localized nonlinear absorption, ultrafast laser processing has a unique 3D spatial selectivity when applied to transparent materials, and appears especially suitable for creating functional optical design and 3D integrated photonics devices [1-6].

In this context, the minimum feature size and the spatial resolution are key factors for ultrafast laser structuring and have a paramount influence on the function that results from the structured material. The minimum feature size is seen here as direct consequence of far-field laser irradiation and the spatial resolution as the critical distance between two structural features without presenting inter-correlation effects. Minimal feature sizes are equally involved in laser-triggered self-organization effects where evanescent near-field light patterns become the driving mechanisms [7]. With respect to minimum feature size, current strategies rely heavily on optical beam engineering to drive the light confinement and the material transformation to the smallest feature size. For instance, relying on threshold effects on Gaussian beam profiles for surface processing, on combining far and near-field effects, or on light-driven self-organization processes [8-12], direct nano-scratching and nano-peeling with feature size in tens of nanometer on target surface were demonstrated. In the bulk as well, self-organization can achieve periodic nanostructures with extreme sizes in the tens of nm range [13]. Achieving similar scales in direct focusing is of interest for enhancing the flexibility of laser treatment. The question of resolution limits is relevant and it intricates light and material reactions. If in ablative ranges on surfaces the minimal size is determined solely by the distribution of input energy [12], a direct nanoscale structuring process in the volume is more complex due to a range of nonlinear physical processes impeding or enhancing the strong localization of light and the strength of the energy gradients. Present scenarios of volume extreme structuring couple nonlinear propagation and thermomechanical evolution, and involve stress-induced cavitation to define minimal achievable sizes [14]. They impact both the minimal feature size and the minimal distance between structures that avoids cross-talk.

This complexifies in consequence the corresponding application of laser pulses in 3D nanostructuring and requires an accurate control of the beam spatial and temporal character during propagation. The proposed solution consists in utilizing a threshold effect for laser-induced microexplosion which occurs under nonequilibrium condition driven by tight laser confinement [15-17]. The achievable energy concentration profiles can be defined using

pulse duration and focusing strength as control knobs. Such an irradiation leads to the creation of nanoscale voids space-selectively inside transparent materials [18], where the nanoscale originates from material expansion under energy gradients provided by light. This technique was recently extrapolated to nondiffractive beams capable of enabling favorable geometries for microexplosions and material cavitation in quasi one-dimensional geometries [19-21], providing feature sizes in the 100 nm range. Overall, with the strong 3D spatial selectivity and potential subwavelength-scale processing capability, such strategy demonstrates significant potential in fabricating size-dependent functions and 3D integrated devices, attracting a particular attention in the recent years [22-25]. High-performance waveguide Bragg gratings [26, 27] and spectro-interferometers [28] based on selective insertion of nanovoids were successfully demonstrated. Nevertheless, different from the performance achieved in shrinking minimum feature size below the 100 nm range, a tenth of the incident wavelength, the resolution limits achievable by this irradiation strategy are not clearly evaluated. The minimum distance between adjacent voids achieved in experiments, free of mutual interferences, remains in the laser-wavelength range. To handle this issue, i.e. to improve the processing spatial resolution, intensive research on ultrafast laser inducing void seems therefore necessary.

Considering that void formation and the characteristic scales rely on the material response to laser excitation, in this work we determine the action range of irradiation. We focus on the morphology characterization of the laser irradiated region in different propagation planes, aiming to obtain information about hydrodynamic and thermodynamic material evolution, their relaxation geometry, and their particular field of action. Then, we identify key factors which restrict the spatial resolution of ultrafast laser structuring and we propose solutions to improve the accuracy. An ultrafast Bessel beam with controllability in geometry and dispersion is used to provide the confined optical field, steering the material reaction in the experiment.

2. EXPERIMENT

A. Ultrafast Bessel beam structuring

An ultrafast Bessel beam in a single-shot exposure mode is used to selectively induce high-aspect-ratio nanovoids gradually penetrating the upper surface of a fused silica (Corning 7980-5F) sample as depicted in Fig. 1(a). The laser source used in the experiment is a Yb:KGW ultrafast laser system (Pharos, Light Conversion) which launches laser pulses with duration tunable in the 290fs-10ps range at a central wavelength of 1030 nm. An axicon lens with a base angle of 1° is used to convert the incoming Gaussian beam into a zeroth order Bessel beam. A 4f system is used to further demagnify and deliver the Bessel beam onto the silica target. The final Bessel beam after imaging 4f system has a half-cone angle of 19.5° in air (13.4° inside silica). The full width at half-maximum of the final Bessel core is calculated to be about 1.11 μm, while the nondiffractive length in air is about 300 μm (460 μm inside silica). The depth of the Bessel beam immersed inside silica, which has determinant influence on the aspect ratio of the nanovoid, is controlled precisely by using a high-precision air-bearing stage (Aerotech ANT 130).

B. Characterization of laser modification

The sample surface structured by the ultrafast Bessel beam is characterized using a scanning electron microscopy (SEM, Helios G4 CX) as shown in Fig. 1(b), aiming to get the characteristics of material reactions on the sample interface. Then the structured sample is milled with using an ion beam source (Leica EM RES102). To suppress the potential additional changes to material surface, the sample is kept at a reduced temperature of tens of degrees Celsius and rotating during milling process, meanwhile, the ion beam is set at a grazing incidence angles (5°) with low average current (2.7 mA), making sure the sample surface skin layer with a thickness of about 5 μm was removed gently. Therefore, such milling process is more like a gentle surface polishing, the influences to the surface micro-structure could be neglected. The laser structured surface after milling process is characterized by scanning electron microscopy, as shown in Fig. 1(c), aiming to get the characteristics of material reactions beneath sample surface. For obtaining a cartography of the material modification range beneath surface, the milled sample is further etched in 5% aqueous solution of hydrofluoric acid for 30 s, and characterized using the scanning electron microscope, as shown in Fig. 1(d). Since fused silica has a poor electrical conductivity, an ion sputter device (Hitachi MC1000) is used to deposit a thin platinum coating on the sample surface to avoid charge build-up during etched morphology characterization. Here it is to be noted that, to avoid the influence of platinum coating on acid etching, the sample is milled again with using the ion beam before etching process.

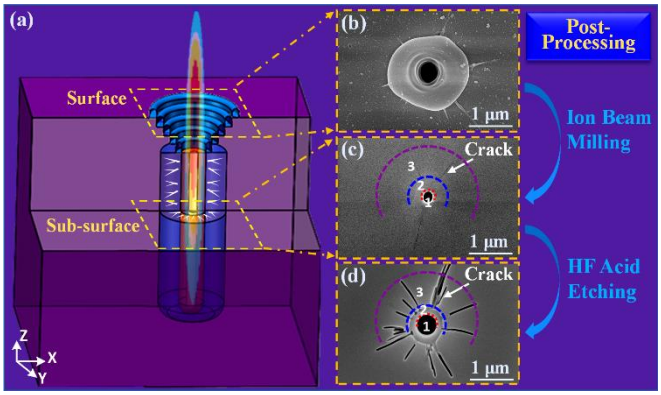

Fig. 1. Schematic diagram of ultrafast Bessel beam irradiation inducing high–aspect-ratio nanovoids penetrating the silica upper surface and the corresponding characterization strategy. (a) section diagram of material reactions within the laser irradiated region, (b) silica surface structured by 1.5 ps ultrafast Bessel pulse with a peak intensity of 1.27×10^{13} W/cm^2 on the upper surface, (c) morphology of nanovoids beneath silica surface (obtained after ion beam milling), (d) morphology of nanovoids beneath silica surface and adjacent regions after acid etching.

3. RESULTS AND DISCUSSION

A. Material reaction trajectory during laser structuring

The demagnified ultrafast Bessel beam with a pulse energy of 13 μJ and pulse duration of 1.5 ps is delivered onto the fused silica. By precisely controlling the focus position, about one-third of the nondiffractive length (92 μm) is immersed inside the silica. The peak intensity (I) is evaluated at 1.27×10^{13} W/cm^2 on the silica upper surface. Since the surface ablation threshold of fused silica is measured to be about 2.4×10^{12} W/cm^2 (for 1.5 ps irradiation), only the central core of the Bessel beam with a higher peak- intensity can trigger the material excitation and structural modification, as illustrated in Fig. 1(a), with the low intensity surrounding rings

leaving no visible trace. Considering that intense energy deposition also proceeds inside the sample along the central lobe formed by conical interference of the incoming fields, strong thermodynamic and hydrodynamic behaviors will emerge triggering the volumetric opening of the void and diffusing in the neighbouring regions [29]. The formation of an energy deposition channel in the bulk that relaxes laterally determines the generation of a void in a narrow region that seems decorrelated from the incident wavelength. The current scenarios indicate as mechanisms pressure or stress-triggered micro explosion and cavitation in either solid or soft phases [15, 20, 30] with a radial relaxation geometry. A mechanical material rupture defines the characteristic nm-range.

The typical appearance of the region depends on the light penetration depth and several planes are analyzed below. On the surface (Fig. 1(b)), as seen by SEM, a standard ablation process overlaps to the bulk void initiation, and the surface through opening delivers an auxiliary pressure relief path pushing away an incipient liquid phase. The presence of liquid in a μm range encompasses the void opening.

The corresponding SEM image of the laser modified region in the subsurface region after ion beam milling process, as shown in Fig. 1(c), reflects a different reaction scenario of material evolution beneath the surface. According to the difference in the morphological characteristics, the laser modified region is divided here into three zones along the radial direction, indicated by dotted lines circles. The zone 1, as circled by red line, corresponds to the nanovoid induced in the center of laser irradiated region. The diameter of nanovoid is measured to be about 290 nm which is consistent with the calculated value by employing energy conservation law [20], and is much smaller than that observed on the silica surface. The zone 2, as encircled between the red line and the blue line, corresponds to the laser excitation region, and has a size close to the Bessel core. Normally, the materials in this region would experience the exposure to photons, local energy absorption, and, in addition, eventual thermomechanical evolutions originated from the void-resulting source. However, no apparent crack is found within this zone. The zone 3, as circled between the blue line and the purple line, locates outside the laser irradiated region, and has a lateral size of more than 2 μm. In contrast to that in zone 2, apparent nanocracks in radial direction were formed in this zone. The existence of nanocracks in zone 3 reflects therefore two points. First, the laser induced mechanical stress inside silica exceeds indeed the critical mechanical strength; while, second, the materials within zone 3 keeps in the solid phase during and after fracture formation. In addition, with respect to the observation that no crack exists in zone 2, this appear to act as a buffer and we believe that laser-induced local melting or at least the rapid onset low-viscosity state should be the main reason. Hence the zone 2 exhibits an annealing region protecting the laser structuring region from mechanical load and failure.

Based on the above observations, aiming to give a description of the stress scenario during laser structuring, the formalism described in Beuton et al. [31] is adopted. The intense energy deposition within the laser excitation region would induce a local high temperature and pressure, triggering the emission of pressure waves, thermal diffusion, dilatation and radial stress. Due to the positive Poisson coefficient of fused silica (e.g. a radial pull being accompanied by a transverse opposite constraint), a shear stress will therefore emerge accompanying the radial propagation of compressive and tensile stresses. Considering the weak resistance of the material to shear stress this results in the radial fracture of the rigid materials within the outer region (zone 3). The development of the central cavitation is also initiated during this process. Owing to the influence of the thermal effects, the rigid material within the laser excitation region turns to be in a low-viscosity state, the radial cracks therefore could not exist within the ring-shape annealing region which surrounds the central void.

The milled sample is further etched with using the HF acid, and the morphology is characterized by SEM as shown in Fig. 1(d). Since the etching rate enhances at the defective region, the profile of laser excitation region, i.e. zone 2, emerges through the morphology contrast. A sharp boundary between zone 2 and zone 3 is highlighted. There is still no crack in zone 2, which confirms that the stress-induced fracture did not happen in the annealing zone 2, or at least be erased during the hydrodynamic process. In contrast, lots of hidden cracks with an outward radiation shape emerge in non-excitation region, i.e. zone 3, outlining in morphology the stress effected region during laser structuring. With using the criterion as discussed the S. Reyne's work [32], the stress for inducing cracks is calculated to be in the few GPa range. Considering the zone 2 and zone 3 have a size much larger than that of the central nanovoid, the laser-induced local annealing and stress would play as main critical factors restricting the structuring resolution.

B. The achievable structuring resolution

In order to analyze the influences of local modifications on the structuring resolution achievable with a Bessel beam, several series of nanovoids with different separation distances are produced using the 1.5 ps ultrafast Bessel beam with the parameters discussed above. The diagram is shown in Fig. 2(a). The peak intensity of the irradiation on silica upper surface is fixed at about 1.1×10^{13} W/cm^2.

The morphology of the initial silica surface after laser structuring is characterized by the SEM as shown in Fig. 2(b-d). The surface aspect of the impact points is characterized by a strong hydrodynamic activity with the expulsion of liquid in a region of around 1 μm radius. This region has also experienced low intensity irradiation from the higher order lobes at 1.7 μm and 3.3 μm. As for the traces of surface modifications, it can be seen that strong mutual effects between adjacent splashed liquid domains start to emerge at a separation distance of 1.5 μm. Considering the distance value is larger than the diameter of laser-excitation region (about 1.3 μm on surface) capable of delivering an ablation effect, this mutual effect can be attributed to several factors: (a) the deposition on the surface of liquid traces, (b) possible changes in the absorption properties due to the standard incubation effects and (c) the residual stress constraints and superposition of mechanical effects. When the separation distance is further decreased to be about 0.75 μm, the independent features of the laser-induced nanovoid completely disappear, exhibiting the influences of the local melting, liquid production, and stress under the circumstance of overlapping-shots. For determining the upper range of the mutual influence on the silica surface, the separation distance is further increased to be about 2.2 μm. At this condition, the mutual effects between adjacent nanovoids disappear. This means the influence range of these threshold-reducing effect is below 2.2 μm, suggesting a minimum action range of 1.1 μm consistent with the kinetic evolution of the liquid.

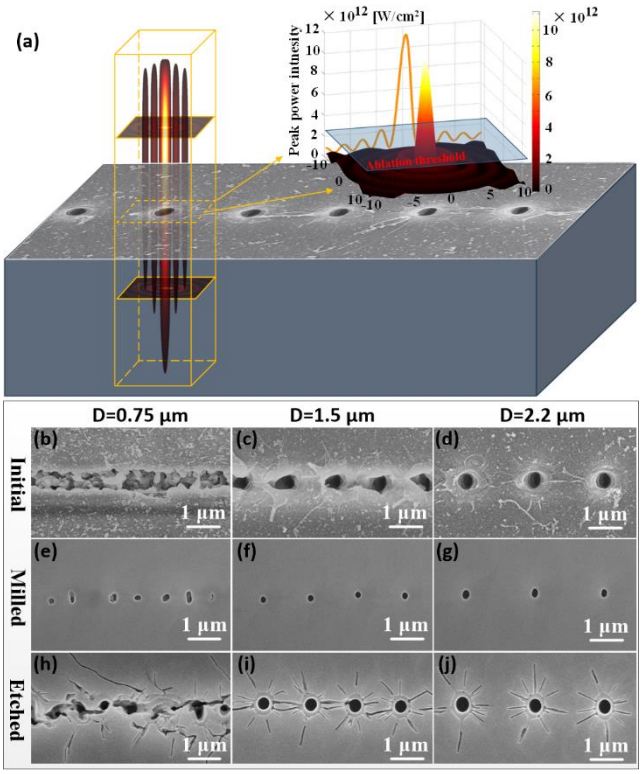

Fig. 2. Series of nanovoids with different separation distance (D=0.75 µm, 1.5 µm, 2.2 µm) induced by 1.5 ps ultrafast Bessel beam of 19.4° cone angle in the single-shot regime. (a) diagram of laser structuring and peak intensity on silica upper surface, (b-d) images correspond to surface successive impacts for different separation distances, (e-g) images correspond to sub-surface impacts for different separation distances, (h-j) images correspond to sub-surface impacts for different separation distances after chemical treatment.

However, beneath the surface the situation appears to be different. The corresponding traces of laser structuring beneath surface are characterized after ion beam milling, as shown in Fig. 2(e-g). For a separation distance of 0.75 µm, the phenomenon is consistent with that on silica surface, the period and independent features of nanovoids are completely distorted. The correlation in the crack orientation suggests a dominant influence of stress and superposition of mechanical effects. However, for a separation distance higher than 1.5 µm, the SEM images show a different situation. Both the period and the feature sizes of the nanovoids are well preserved, even though some cracks have overlapped between the voids. The cracks as discussed before are the consequence of radial stress geometry resulting from the thermal expansion triggered by the central cylindrical heated material [33]. This process indicates that the volume matter inside has a better performance for confining the stress influencing region if a critical distance is maintained. The morphology of the samples after HF acid etching, as shown Fig. 2(h-j), prove well this point. The characterization results in this section reflect that, given its action range compared to local-annealing, the laser-induced stress should be the primary factor in restricting the structuring resolution. The mechanical load creates mutual reinforcements between the stress fields of each void channel, but the void themselves do not obstruct the passage of the conical waves forming the Bessel channels. A possible bypass strategy given the µs time required to propagate stress [31] should then involve simultaneous production of structures using parallel irradiation techniques. We identify below irradiation parameters that can physically contain the material response, concentrating on the annealing (2) and stress (3) domains.

C. Dependence of the local annealing and shock stress on intensity

The dependence of the in-volume local annealing (region 2) and and the residual stress (region 3) on the peak intensity is studied in this section. By varying first the pulse energy, the laser irradiation on silica upper surface is regulated from 3.85×10^{12} W/cm^2 to 1.47×10^{13} at a pulse duration of 1.5 ps. We state that the corresponding intensity in the bulk may follow a different dependence as nonlinear propagation and excitation effects intervene but we may assume a monotonic dependence. The SEM images, as shown in Fig. 3(a), present the morphology of the corresponding laser-structured regions at different layers in depth. It is apparent that there is a relationship between the size of laser-modified region and laser irradiation. The outer diameters of nanovoids, local annealing region (i.e. zone 2, the ring-like region surrounding the void), and residual-mechanical stress (zone 3) effected region decrease with the decrease of peak intensity, as observed in Fig. 3(b-d). This dependence is conceivable from energy conservation considerations. The void volume is defined by the condition that the energy density overcomes the cohesion threshold. This implies a dependence on the volume energy density value within the modified region and on the gradients, therefore the shape. The minimum diameter of nanovoids is characterized to be in the 100 nm range, much smaller that the spot waist, and its volume will be dictated by the energy density value. Given the one-dimensional geometry with the length fixed in space by the non-diffractive distance, the dependence should then follow a quasi square-root dependence with the energy, hence, here with intensity The local annealing region could nonetheless be determined by the energy deposition given by the spatial distribution of intensity (and therefore scaling approximately with its logarithm for a distribution that can be approximated for the region above the threshold by a Gaussian shape). The stress induced cracks beneath the surface seem always to exist around the voids, evidence of the stress, and the minimum outer diameter of the corresponding region is in the micron order. A similar criterion requiring to bypass the material strength can be applied, notwithstanding that bulk peak intensity and thus energy densities can depart from the value reported at the surface. Taken into account these dependencies we will try to fit the results as a function of the equivalent peak intensity in vacuum, which represents in this case a measure of local energy density.

The peak intensity is calculated by the formula $I(r,z) = 8\pi P_0 z sin^2\theta/(\lambda w^2)\exp[-2(ztan\theta/w)^2]\, J_0^2(krsin\theta)$ as used in reference [19], neglecting eventual nonlinearities in propagation, self-focusing and other factors. This is justified to a certain extent by rather tight focusing conditions, where the high convergence angle overcomes diffraction and scattering effects. From the Fig. 3(b) and (d), it can be seen that the dependencies of the diameters of the void and the residual-mechanical stress effected region on peak intensity can be well fitted by $d_i = \beta_i \sqrt{I}$. In addition, the dependence of the diameter of the local annealing region on peak intensity is well fitted by $d = \alpha \ln(I)$, as shown in Fig. 3(c) in this intensity range, reduced nevertheless to infer a more exact dependency.

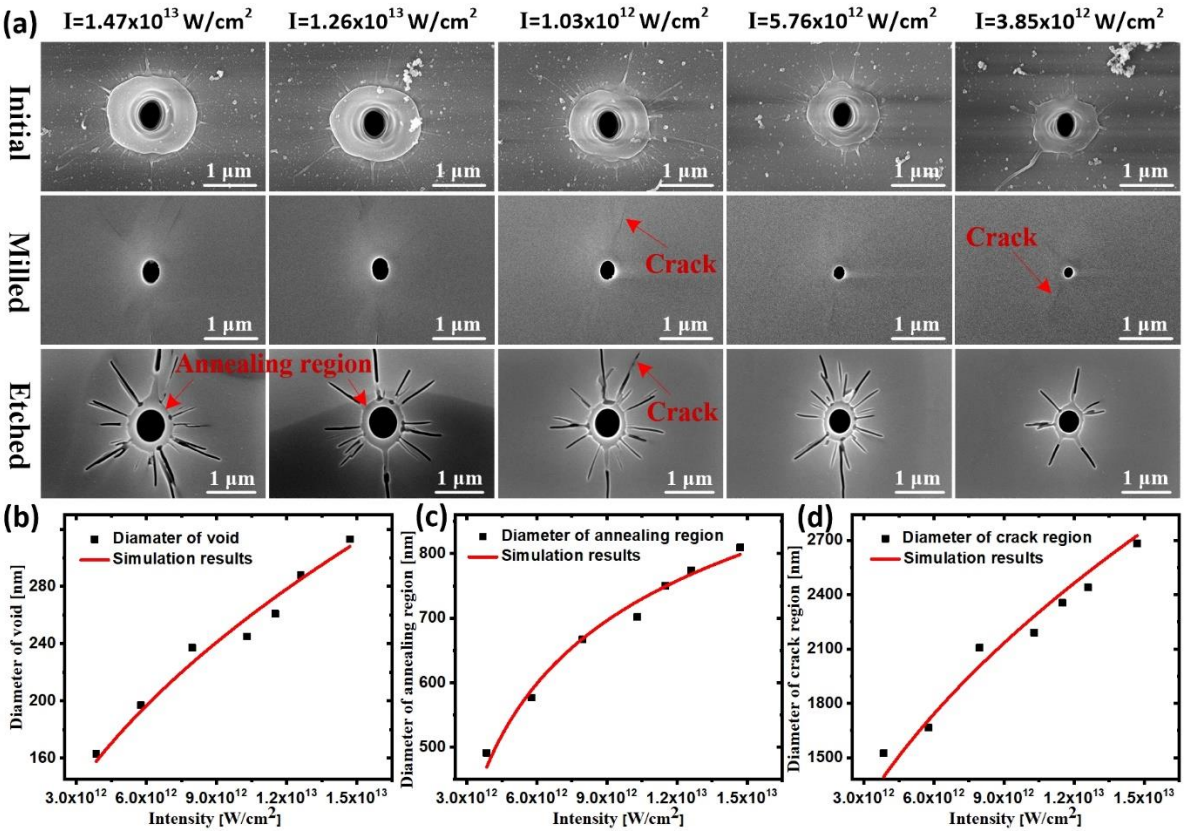

Fig. 3. (a) Nanovoids induced by 1.5 ps ultrafast Bessel beam with different pulse energies and thus intensities, (b) the dependences of the outer diameter of nanovoids measured after milling process on the peak intensity, (c) the dependences of the outer diameter of local annealing region measured after milling and etching process, (d) the dependences of the outer diameter of shock-stress effected region measured after milling and etching process on the peak intensity.

D. Dependence of the local affected zones on pulse duration

The influences of pulse duration on the material responses, including cavitation, the extent of local annealing and the stress-induced fracture, are investigated in this section. The pulse duration is seen here as a control factor for the nonlinear propagation and a possibility therefore to maximize the nonlinear excitation confinement in the bulk. It equally influences the energy absorption in the neighboring regions. The pulse energy in this section is kept at a fixed value of about 13 uJ for different pulse duration. As for 0.2 ps laser irradiation, the corresponding maximum intensity on the silica upper surface is about 9.53×10^{13} W/cm^2. For different pulse durations the SEM images, as shown in Fig. 4, present the morphology of the laser modified regions before and after ion beam milling, and then, to enhance the visibility of the material response, after HF acid etching.

With respect to the characterization results of the initial silica surface after laser structuring, it can be seen that intense surface ablation accompanying material ejection in the liquid phase took place for 0.2 ps ultrafast laser irradiation. When the pulse duration is gradually increased, the phenomenon of material ejection is apparently reduced (Fig. 4(a)), indicating potentially a lower pressure acting on the liquid, as well as a lower yield of surface excitation as the surface intensity drops. After the ion beam milling process, i.e. remove the ablated surface layer, the voids in hundreds-nanometer lateral size are exposed. The excitation yield shows a different dynamics (Fig. 4(b)). The diameter of the void increases around 1.5 ps suggesting a strong mechanical drive for growing the void, signaling an increase in the deposited energy density. The diameter decreases again for higher pulse durations as the excitation intensity and thus the deposited energy density goes down. The remarkable outcome appears also in the analyses of the cracks. For the 0.2 ps and 9.0 ps laser structuring, the extremes of our investigation ranges, it seems that there is no crack formation locating outside the voids. The images of the sample after the acid etching process further conform this point (Fig. 4(c)). With respect to the 1.5 ps, 3.5 ps and 6.0 ps laser structuring conditions, there are apparent nanocracks induced outside the local annealing region, which indicates that the material under this irradiation condition experienced a strong radial expansion under the drive of heat and stress evolution. This equally confirms that, opposite to surface phenomena of liquid ejection, for bulk evolution the volume energy density does not follow the surface intensity trend, being set by a balance of diffraction and carrier-induced scattering and achieving a maximum for intermediate pulse lengths in the 1-2 ps range [31].

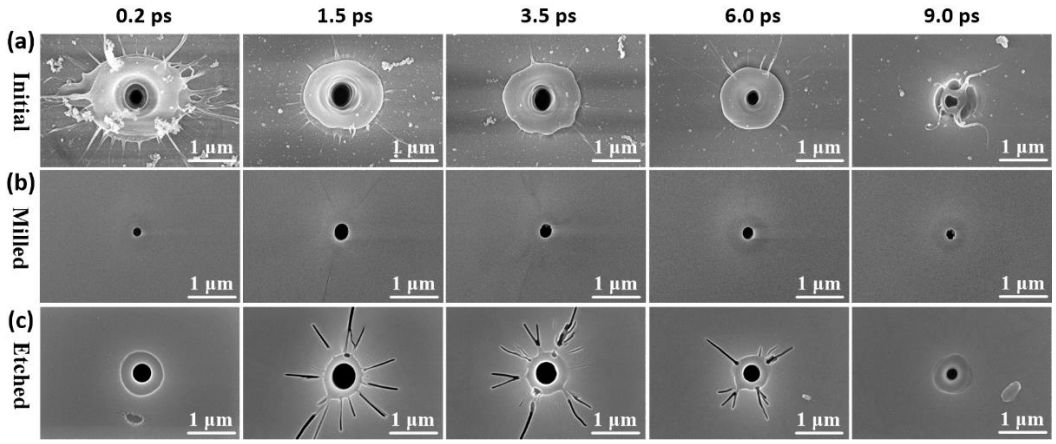

Fig. 4. Influences of the pulse duration on ultrafast laser structuring and the extent of the affected zone: (a) initial surface after irradiated by ultrafast Bessel beam, (b) morphology characterization of the sample after ion beam milling process; sub-surface features, (c) morphology characterization of the sample after acid etching process. The respective pulse durations are indicated on the figure. The pulse energy is kept at a fixed value of about 13 uJ.

In order to perform a careful analysis, the results of Bessel beam structuring as a function of pulse duration are represented in Fig. 5. Guiding eye exponential functions are utilized to fit the experimental data. Fig. 5(a) exhibits the relationship between the void diameter (measured after milling process) and pulse duration. Between 0.2 ps to 1.5 ps, the void diameter increases with the increase of pulse duration for constant energy. This indicates an increase of the energy density within the Bessel channel, making an intermediate pulse value more favorable for inducing voids compared to the shortest pulse value. However, when the pulse duration is further increased to be above 1.5 ps, the void diameter decreases monotonically. The similar phenomenon was also found in previous works using the 800 nm ultrafast laser [29] and explained with a nonlinear beam propagation controlled by laser-induced plasma defocusing scattering the light away from the propagation axis. The loss effect, stronger for short pulse durations results in a lower energy density and thus in a narrower resulting void. The extent of the liquid flow on the surface (Fig. 4(a)) would mean in this context that its origin lays more in a surface ablation process generating also melt rather than ejection of liquid from the underneath crater which should reflect the energy content. In this case the intensity on surface caused by the short pulse Bessel beam well above the surface threshold will cause a more explosive process.

Figure 5(b) presents the relationship between the annealing region (i.e. zone 2, the laser excitation region) and pulse duration. The outer diameter of the annealing region is characterized after milling and etching process. It can be seen that the diameter value exhibit a decay with the increase of the pulse duration. Considering for example the 9.0 ps laser structuring, the diameter of the annealing region is measured to be about 680 nm, much smaller than that for 0.2 ps laser structuring (910 nm). Considering the size of local material annealing zone stays within the profile of the laser excitation, the results presented in Fig. 5(b) also provide supports for the above explanation to some extent. The 1.5 ps pulse will provide a more favorable conversion of energy into mechanical forms, affecting the void, while the annealing region seems consistent with the intensity transverse spatial profile thresholded by a material dependent value. Here we need to note that, even if the annealing region can be well restricted though increasing the pulse duration, the minimum diameter still has a value larger than 500 nm.

Figure 5(c) presents the experiment results of the stress induced fracture (characterized after milling and etching process). Similar to that in Fig. 5(a), there is no simple linear relationship between the diameter of cracked region and the pulse duration. In the range of 0.2 ps to 1.5 ps, the diameter increases with the increase of pulse duration, and reaches maximum of about 2500 nm at 1.5 ps. When the pulse duration is further increased to be above 1.5 ps, the diameter of the stress affected zone decreases. We note then the correlation between the void and the stress range evolution. These experimental results reflect that the mechanical stress induced fracture is also sensitive to the pulse duration, and the density of the deposited laser energy should be the main reason. Here we would like to note that, the diameter value at pulse duration of 0.2 ps and 9.0 ps are equal to that of the outer diameter of the annealing region, this means there is no crack formation under the corresponding laser structuring condition, with perhaps a decrease in the local stress considering the size of the corresponding void. Based on the results above, aiming to suppress the crack formation during laser structuring, the shortest or relatively long temporal duration laser seem more efficient in avoiding excessive density of the deposited energy. This indicates on one hand that shortest pulse regulates nonlinearly the energy concentration to minimize heat excursions, as seen also for the longer pulse value where only the intensity-dependent nonlinear excitation cross-section drops significantly. A second factor can be related to the rapid establishment of a low viscosity layer around, damping efficiently the evolving stress fields.

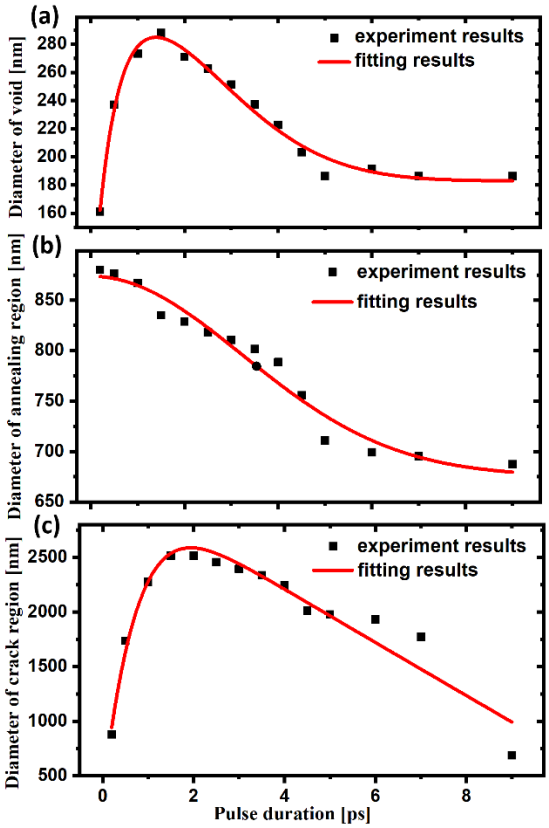

Fig. 5. Experimental data and eye-guiding fitting results of Bessel beam structuring as a function of pulse duration: (a) the void diameter, (b) the diameter of the local annealing region, (c) the diameter of the crack region.

E. Femtosecond laser structuring without inducing nanocracks

The resistance to cracking and thus to stress constraints is critical for volume error-free processing. As a demonstration, the single-shot laser structuring is performed with using the shortest duration of the pulsed laser. By controlling the pulse energy, the peak intensity on silica upper surface is regulated in a domain ranging from 7.33×10^{13} W/cm^2 to 4.03×10^{13} W/cm^2. The SEM images, as shown in Fig. 6, presents the morphology of the laser modified region before and after ion beam milling and then after the contrast enhancement via chemical etching. It is apparent that intense material ejection is induced on the silica surface after laser irradiation. Both the diameters of nanovoid, local annealing region and liquid-flow region decrease monotonously with the decrease of peak intensity via the energy change. This suggest at the first hand less kinetic energy for the ejecta, less inner pressure build-up and release in the bulk in the radial geometry, as well as a lesser dose in the neighboring regions. The minimum diameters of the nanovoid achieved in the experiment are 123 nm, with a local annealing range of 620 nm, respectively. No apparent nanocrack is found within the laser modified region.

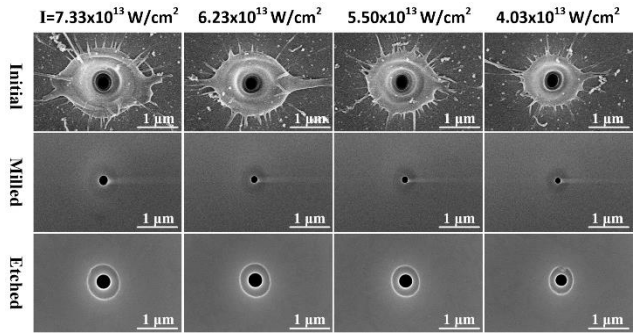

Fig. 6. Femtosecond laser structuring performed with different peak intensity ranging from 7.33×10^{13} W/cm^2 to 4.03×10^{13} W/cm^2 showing surface and bulk pulse action ranges. An ultrashort pulse duration is used, generating crack-free volume.

4. CONCLUSION

In conclusion, multiple morphological characterization aspects of the material responses on the surface and sub-surface regions triggered during laser structuring were performed under the assistance of ion beam milling and HF acid etching. According to the difference in morphological characteristics, the laser modified region beneath surface was divided into three zones with radial geometries, cavitation region, local annealing region, and crack formation region, respectively, while liquid domains were observed on the surface. The crack formation region had a typical lateral size on the micron order, meanwhile the void lateral size was on ~100 nm order, surrounded by a narrow annealing ring-like region. Based on their extended action range, the laser induced local annealing and mechanical stress were considered be the crucial factors restricting the laser structuring resolution. Their influence is mainly manifested by enhancing distance-dependent cooperative material effects and not by obstacles to the laser light. The peak intensity and pulse duration were demonstrated to be able to regulate the material responses, including local annealing and residual stress. Interestingly, the local annealing and mechanical stress exhibited different reaction behaviors with respect to pulse duration, emphasizing volume nonlinear effects triggering a delicate balance of mechanical and thermal effects. For restricting the influences of local annealing and mechanical stress during laser structuring outside the excitation region, it seems better to utilize the laser with either short or relatively long temporal duration.

CRediT authorship contribution statement

Guodong Zhang: Investigation, Results analyzation, Writing original draft, Methodology. Razvan Stoian: Results analyzation, Writing original draft. Rui Lou: Conceptualization, Writing review & editing. Tianqu Chen: Conceptualization, Writing review & editing. Guangying Li: Conceptualization, Writing review & editing. Xu Wang: Writing review & editing. Yan Pan: Methodology, Writing review & editing. Pengfei Wu: Methodology, Writing review & editing. Jiang Wang: Methodology, Writing review & editing. Guanghua Cheng: Results analyzation, Writing - review & editing, Supervision, Project administration, Funding acquisition.

Declaration of Competing Interest:

The authors declare that they have no known competing financial interests or personal relationships that could have appeared to influence the work reported in this paper.

Acknowledgment.

The research work was supported by the National Key Research and Development Program of China (2018YFB1107401), Natural National Science Foundation of China (61775236). We would like to thank the Analytical &Testing Center of Northwestern Polytechnical University for Ion beam milling and SEM characterization.

References

1. Y. Cheng, K. Sugioka, K. Midorikawa, M. Masuda, K. Toyoda, M. Kawachi, and K. Shihoyama, "Three-dimensional micro-optical components embedded in photosensitive glass by a femtosecond laser," Optics Letters **28**(13), 1144-1146, (2003).
2. Y. Liao, J. Song, E. Li, Y. Luo, Y. Shen, D. Chen, Y. Cheng, Z. Xu, K. Sugioka, and K. Midorikawa, "Rapid prototyping of three-dimensional microfluidic mixers in glass by femtosecond laser direct writing," Lab on a Chip **12**(4), 746-749, (2012).
3. E. N. Glezer, M. Milosavljevic, L. Huang, R. J. Finlay, T. H. Her, J. P. Callan, and E. Mazur, "Three-dimensional optical storage inside transparent materials," Optics Letters **21**(24), 2023-2025, (1996).
4. I. Spaleniak, S. Gross, N. Jovanovic, R. J. Williams, J. S. Lawrence, M. J. Ireland, and M. J. Withford, "Multiband processing of multimode light: combining 3D photonic lanterns with waveguide Bragg gratings," Laser & Photonics Reviews **8**(1), L1-L5, (2014).
5. R. R. Thomson, T. A. Birks, S. G. Leon-Saval, A. K. Kar, and J. Bland-Hawthorn, "Ultrafast laser inscription of an integrated photonic lantern," Optics Express **19**(6), 5698-5705, (2011).
6. S. Mukherjee, A. Spracklen, M. Valiente, E. Andersson, P. Ohberg, N. Goldman, and R. R. Thomson, "Experimental observation of anomalous topological edge modes in a slowly driven photonic lattice," Nature Communications **8**, 13918, (2017).
7. J. E. Sipe, J. F. Young, J. S. Preston, and H. Driel, "Laser-Induced Periodic Surface Structure. I. Theory," Physical review. B, Condensed matter **27**(2), 1141-1154, (1983).
8. V. R. Bhardwaj, E. Simova, P. P. Rajeev, C. Hnatovsky, R. S. Taylor, D. M. Rayner, and P. B. Corkum, "Optically produced arrays of planar nanostructures inside fused silica," Physical Review Letters **96**(5), 057404, (2006).
9. Z. Lin, H. Liu, L. Ji, W. Lin, and M. Hong, "Realization of similar to 10 nm Features on Semiconductor Surfaces via Femtosecond Laser Direct Patterning in Far Field and in Ambient Air," Nano Letters **20**(7), 4947-4952, (2020).
10. Z. Z. Li, L. Wang, H. Fan, Y. H. Yu, Q. D. Chen, S. Juodkazis, and H.-B. Sun, "O-FIB: far-field-induced near-field breakdown for direct nanowriting in an atmospheric environment," Light: Science & Applications **9**(1), 41, (2020).
11. A. P. Joglekar, H. H. Liu, E. Meyhofer, G. Mourou, and A. J. Hunt, "Optics at critical intensity: Applications to nanomorphing," Proc Natl Acad Sci U S A **101**(16), 5856-5861, (2004).
12. M. Garcia-Lechuga, O. Utéza, N. Sanner, and D. Grojo, "Evidencing the nonlinearity independence of resolution in femtosecond laser ablation," Optics Letters **45**(4), 952-955, (2020).
13. Y. Shimotsuma, P. G. Kazansky, J. R. Qiu, and K. Hirao, "Self-organized nanogratings in glass irradiated by ultrashort light pulses," Physical Review Letters **91**(24)(2003).
14. R. Stoian and J.-P. Colombier, "Advances in ultrafast laser structuring of materials at the nanoscale," Nanophotonics **9**(16), 4665-4688, (2020).
15. S. Juodkazis, K. Nishimura, S. Tanaka, H. Misawa, E. G. Gamaly, B. Luther-Davies, L. Hallo, P. Nicolai, and V. T. Tikhonchuk, "Laser-Induced Microexplosion Confined in the Bulk of a Sapphire Crystal: Evidence of Multimegabar Pressures," Physical Review Letters **96**(16), 166101, (2006).
16. L. Rapp, B. Haberl, C. J. Pickard, J. E. Bradby, E. G. Gamaly, J. S. Williams, and A. V. Rode, "Experimental evidence of new tetragonal polymorphs of silicon formed through ultrafast laser-induced confined microexplosion," Nature Communications **6**, 7555, (2015).
17. S. Juodkazis, H. Misawa, T. Hashimoto, E. G. Gamaly, and B. Luther-Davies, "Laser-induced microexplosion confined in a bulk of silica: Formation of nanovoids," Applied Physics Letters **88**(20), 201909, (2006).
18. E. G. Gamaly, S. Juodkazis, K. Nishimura, H. Misawa, and B. Luther-Davies, "Laser-matter interaction in the bulk of a transparent solid: Confined microexplosion and void formation," Physical Review B **73**(21), 214101, (2006).
19. M. K. Bhuyan, F. Courvoisier, P. A. Lacourt, M. Jacquot, R. Salut, L. Furfaro, and J. M. Dudley, "High aspect ratio nanochannel machining using single shot femtosecond Bessel beams," Applied Physics Letters **97**(8), 081102, (2010).
20. M. K. Bhuyan, M. Somayaji, A. Mermillod-Blondin, F. Bourquard, J. P. Colombier, and R. Stoian, "Ultrafast laser nanostructuring in bulk silica, a “slow” microexplosion," Optica **4**(8), 951-958, (2017).
21. Z. Wang, L. Jiang, X. Li, A. Wang, Z. Yao, K. Zhang, and Y. Lu, "High-throughput microchannel fabrication in fused silica by temporally shaped femtosecond laser Bessel-beam-assisted chemical etching," Optics Letters **43**(1), 98-101, (2018).
22. R. Stoian, M. K. Bhuyan, A. Rudenko, J. P. Colombier, and G. Cheng, "High-resolution material structuring using ultrafast laser non-diffractive beams," Advances in Physics: X **4**(1), 1659180, (2019).
23. K. Sugioka and Y. Cheng, "Femtosecond laser three-dimensional micro- and nanofabrication," Applied Physics Reviews **1**(4), 041303, (2014).
24. Y. Shimotsuma, K. Hirao, P. G. Kazansky, and H. R. Qiu, "Three-dimensional micro- and nano-fabrication in transparent materials by femtosecond laser," Japanese Journal of Applied Physics Part 1-Regular Papers Brief Communications & Review Papers **44**(7A), 4735-4748, (2005).
25. A. Rodenas, M. Gu, G. Corrielli, P. Paie, S. John, A. K. Kar, and R. Osellame, "Three-dimensional femtosecond laser nanolithography of crystals," Nature Photonics **13**(2), 105-109, (2019).
26. G. Zhang, G. Cheng, M. Bhuyan, C. D'Amico, and R. Stoian, "Efficient point-by-point Bragg gratings fabricated in embedded laser-written silica waveguides using ultrafast Bessel beams," Optics Letters **43**(9), 2161-2164, (2018).
27. G. Zhang, G. Cheng, M. K. Bhuyan, C. D’Amico, Y. Wang, and R. Stoian, "Ultrashort Bessel beam photoinscription of Bragg grating waveguides and their application as temperature sensors," Photon. Res. **7**(7), 2327-9125, (2019).
28. G. Martin, M. Bhuyan, J. Troles, C. D'Amico, R. Stoian, and E. Le Coarer, "Near infrared spectro-interferometer using femtosecond laser written GLS embedded waveguides and nano-scatterers," Optics Express **25**(7), 8386-8397, (2017).
29. M. K. Bhuyan, P. K. Velpula, J. P. Colombier, and T. Olivier, "Single-shot high aspect ratio bulk nanostructuring of fused silica using chirp-controlled ultrafast laser Bessel beams," Applied Physics Letters **104**(2), 219-377, (2014).
30. M. Somayaji, M. K. Bhuyan, F. Bourquard, P. K. Velpula, C. D'Amico, J.-P. Colombier, and R. Stoian, "Multiscale electronic and thermomechanical dynamics in ultrafast nanoscale laser structuring of bulk fused silica," Scientific Reports **10**(1), 15152, (2020).
31. R. Beuton, B. Chimier, J. Breil, D. Hebert, P.-H. Maire, and G. Duchateau, "Thermo-elasto-plastic simulations of femtosecond laser-induced structural modifications: Application to cavity formation in fused silica," Journal of Applied Physics **122**(20), 203104, (2017).
32. S. Reyné, G. Duchateau, L. Hallo, J. Y. Natoli, and L. Lamaignère, "Multi-wavelength study of nanosecond laser-induced bulk damage morphology in KDP crystals," Applied Physics A **119**(4), 1317-1326, (2015).
33. R. Beuton, B. Chimier, P. Quinoman, P. González Alaiza de Martínez, R. Nuter, and G. Duchateau, "Numerical studies of dielectric material modifications by a femtosecond Bessel–Gauss laser beam," Applied Physics A **127**(5), 334, (2021).